A simplified analytical method for predictions of ship deckhouse collision loads on steel bridge girders

Yanyan Sha[a*] and Jørgen Amdahl[a]

[a]*Centre for Autonomous Marine Operations and Systems, Department of Marine Technology, Norwegian University of Science and Technology, Otto Nielsons Vei 10, Trondheim 7491, Norway*

*corresponding author: Yanyan Sha. E-mail: yanyan.sha@ntnu.no

A simplified analytical method for predictions of ship deckhouse collision loads on steel bridge girders

Bridges across busy navigation channels are under the threat of accidental ship collisions. Many research works have been conducted to investigate the structural responses during ship bow-bridge pier collisions. However, the collisions between the ship deckhouse and the bridge girder have not been well studied. In this paper, a container ship deckhouse impact with a floating bridge girder is investigated. High fidelity finite element models of a ship deckhouse and a bridge girder are developed. The impact demand and the structural deformation during the deckhouse-girder collision are numerically obtained. Based on the deformation mechanism observed from the simulation, a simplified analytical method is proposed for the fast prediction of the impact force and energy dissipation. The analytical method derives expressions to estimate the impact resistance of the major structural components in the ship deckhouse, and the total resistance and energy absorption are obtained by adding up the contributions from the individual structural components. The impact resistance and energy dissipation calculated by the simplified analytical method are validated against the numerical results for various collision scenarios. Results show the proposed method can accurately and efficiently estimate the impact demand of deckhouse-girder collisions.

Keywords: analytical approach; deckhouse collision; bridge girder

Introduction

Due to the increasing demand for transportation, a growing number of large-scale bridges have been designed and constructed in the past decades. Meanwhile, the probability of ship collision with bridge structures has also increased significantly. Special attention has been paid to predict the impact demand and evaluate the structural response for ship bow collision with bridge substructures. However, apart from such collisions, the collision accidents between the superstructures of ships and bridges have also increased dramatically.

Depending on the ship draught and the girder clearance, ship-bridge superstructure collisions can be divided into two main categories, i.e., ship forecastle collision with bridge girders and ship deckhouse collision with bridge girders. The responses of forecastle-girder collisions and deckhouse-girder collisions are quite different due to the geometrical and strength differences in ship forecastles and deckhouses (Sha et al. 2018). Some preliminary studies have been conducted to investigate the impact response of floating bridge girder under ship forecastle collisions (Sha and Amdahl 2016, Sha and Amdahl 2017). However, the literature on the estimation of the impact demand and the structural response of ship deckhouse collisions is quite limited. Hence, it is important to carry out such studies to better design the structures for such accidents.

The literature on the estimation of collision force from ship deckhouse impacts with bridge superstructures is very limited. Pedersen et al. (1993) pointed out that the deckhouse impact force highly depends on the contact height which is directly related to the girder geometry (see Figure 1). Based on the investigation conducted in the Great Belt Bridge project, it was recommended that design deckhouse impact loads should be calculated depending on the size of the contact area, i.e. the product of the contact height and the breadth of the deckhouse. The deckhouse impact loads on bridge superstructures should be obtained from the loads required to deform the structural elements of the deckhouse. However, variations of the girder geometry and deckhouse configuration were neglected. Moreover, the study was conducted for concrete bridge girders that were assumed to remain virtually undamaged by the impact. For steel bridge girders, the interaction between girder and deckhouse may be important.

Sha and Amdahl (2018) developed finite element models of a steel bridge girder and a container ship deckhouse. Numerical simulations were conducted to obtain the

impact force during deckhouse-girder collisions. The effort related to model development and numerical simulations was extensive and the obtained impact force was only applicable to the specific ship deckhouse and the bridge girder. For a quick estimation of deckhouse-girder impact load in the preliminary bridge design phase, a simple, yet reasonably accurate method should be developed.
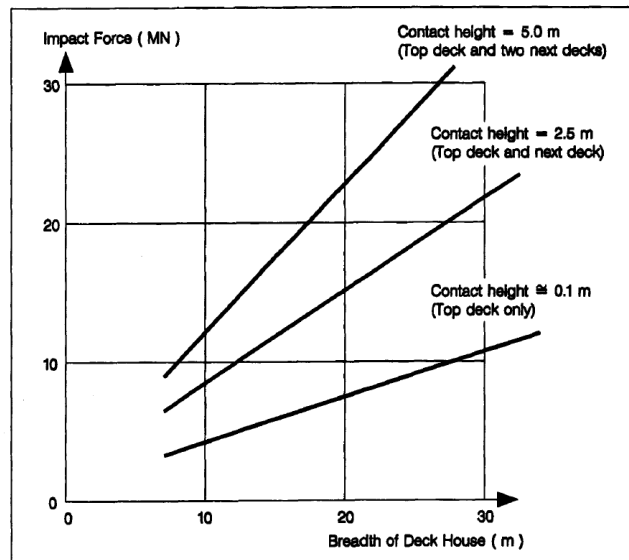

Figure 1. Impact force chart for deckhouse collision with bridge superstructures (Larsen 1993).

Simplified analytical methods to assess the damage and energy dissipation during collisions and grounding have been developed by many researchers (Hong and Amdahl 2008, Hong and Amdahl 2012, Liu 2017, Sha and Hao 2014, Sun et al. 2015, Sun et al. 2017, Zhang and Pedersen 1999). The energy conservation law and plastic theory are commonly used to estimate the impact resistance and energy absorption of various structural components. The total energy dissipated by the structure is obtained by adding up the contributions of all structural components engaged in the collision.

In a deckhouse-girder collision, the edge of the steel bridge girder imposes typically a line load with a length equals to the width of the deckhouse. This loading pattern differs from those of the collision and grounding studies which focused on

stiffened plates subjected to concentrated loads from various indenters (round, cylinder and wedge-shaped etc.).

In this paper, finite element models of a ship deckhouse and a section of bridge girder are developed. Numerical simulations are first conducted to investigate the collision response of deckhouse-girder collisions. Based on the deformation mechanism, a simplified analytical approach is developed. It predicts the structural resistance and energy dissipation of the deckhouse by assembling the contributions of the major structural components. The method is validated against the results from numerical simulations with high-resolution FE models.

Finite element models

Finite element models of the ship deckhouse and the bridge girder are established for explicit numerical simulations conducted with the software package LS-DYNA.

Ship deckhouse FE model

The ship deckhouse model is based on a container ship with has a total length of 166 m and a beam width of 22.5 m. In this study, the structures in the deckhouse were modelled in detail to accurately represent the structural strength. This is because only the deckhouse is expected to be in direct contact with the bridge girder and thus an accurate modelling of this part is required. The ship body was simply modelled by very coarse rigid shell elements to illustrate the shape and the dimension of the ship. As shown in Figure 1, the ship hulls, internal decks, girders and stiffeners were carefully modelled using four-node shell elements. The plate thickness of the deckhouse and internal structures varies from 7 mm to 18 mm. A general mesh size of 100 mm was used. The main dimensions of the deckhouse are illustrated in Figure 2.
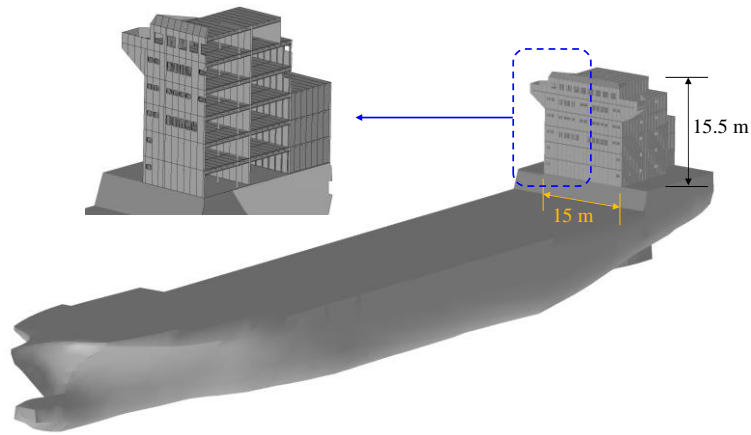
Figure 2. FE model of the container ship.

Girder FE model

The bridge girder model used in this study was developed based on the prototype of a steel girder in a continuous floating bridge. The cross-sectional dimensions of the girder are shown in Figure 3. The girder top plate is 14 mm thick while the other plates are 12 mm thick. The transverse diaphragms have a spacing of 4 m and the thickness of the diaphragm web and flange is 12 mm. In the longitudinal direction, the girder plates are supported by hat stiffeners with a thickness ranging from 6 mm to 10 mm as shown in the figure. Vertically, 6.3 mm thick hollow circular trusses with a diameter of 219 mm are connected to diaphragms through welding plates. The beam trusses are connected to the shell diaphragms at several points so as to avoid local overloading of a shell element. In total, 14 sections (56 m) of the bridge girder were modelled as shown in Figure 3. The same mesh size of 100 mm was used in the bridge girder as that in the deckhouse.
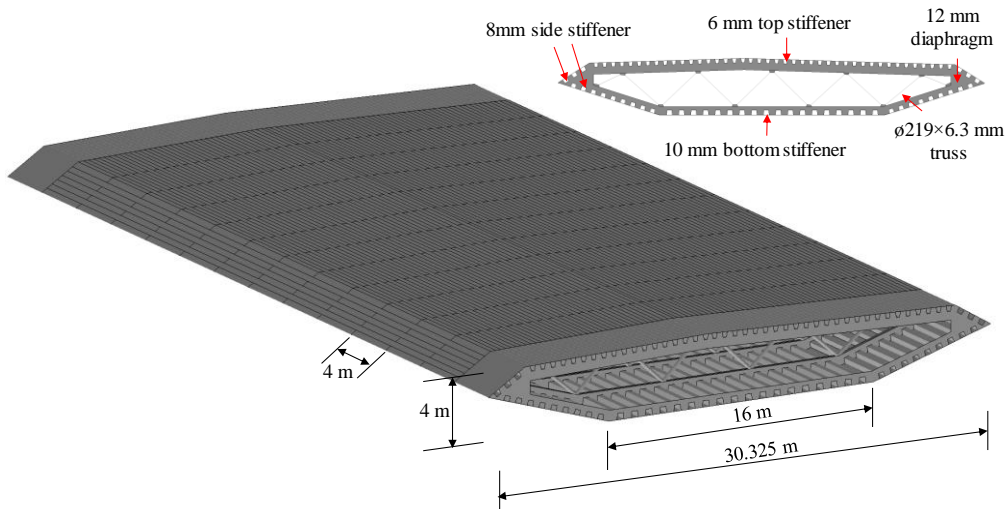
8mm side stiffener 6 mm top stiffener 12 mm diaphragm

10 mm bottom stiffener ø219×6.3 mm truss

4 m

4 m

16 m

30.325 m

Figure 3. Finite element model of the bridge girder section.

Material modelling

For the material modelling, a power-law hardening model was used for the steel material in this study (Alsos et al. 2009). The material was assumed to have isotropic plastic properties and modelled using plane stress J2 flow theory. The equivalent stress-strain curve is represented by a modified power-law formulation includes a plateau strain. The Rice-Tracey-Cockcroft-Latham criterion (RTCL) is used to model material failure (Alsos, Amdahl and Hopperstad 2009). It considers stress triaxiality to separate between shear and tension dominated damages. The ship deckhouse is constructed of mild steel while the bridge girder is made of high-strength steel. The characteristic yield stresses for the deckhouse and the girder are 270 MPa and 420 MPa respectively. The material parameters are tabulated in Table 1 and the stress-strain curves are plotted in Figure 4.

Table 1. Material properties.

Parameters	Mild steel (Ship Deckhouse)	High-strength steel (Bridge girder)
Density	7850 kg/m^3	7850 kg/m^3
Young's modulus	206 GPa	206 GPa

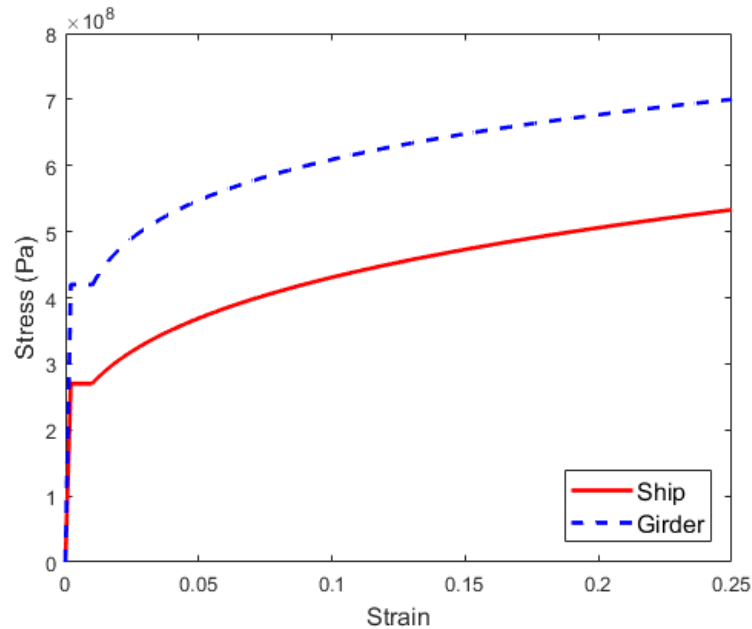|		
Poisson's ratio	0.3	0.3
Yield stress	270 MPa	420 MPa
Strength index (K)	740 MPa	863 MPa
Strain index (n)	0.24	0.15

Figure 4. True stress-strain curves for the steel material in the ship and the girder.

Collision setup

Figure 5 shows the setup for deckhouse-girder collision simulations. The deckhouse is assumed to impact at the centre of the girder. In the simulation, the girder is fixed in all degrees of freedom at both ends and the ship collides against the girder with a constant speed of 10 m/s to save the computational time. Any strain rate hardening is not accounted for in this study as this is considered of moderate influence (Storheim and Amdahl 2017). The contact between the striking ship and the struck girder is defined as the Automatic-Surface-to-Surface contact and the internal contacts in the deckhouse and the deck girder are also considered by using the Automatic-Single-Surface contact algorithm. The friction coefficients of both contact types are assumed to be 0.3 (Sha and Hao 2012).
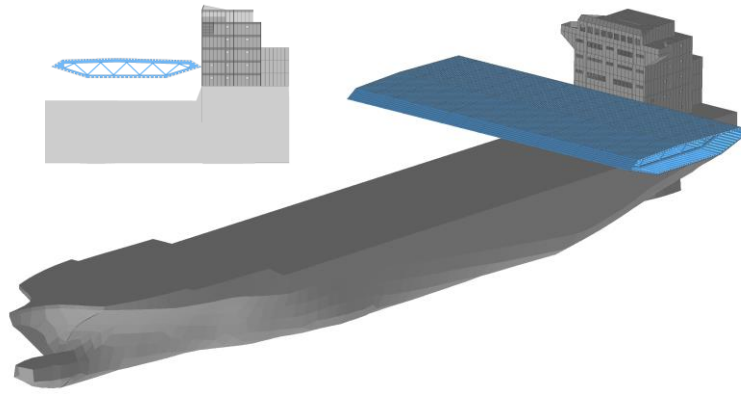
Figure 5. Illustration of the collision setup for the ship and the bridge girder.

Numerical results

Impact response

An integrated analysis, i.e. with both deformable deckhouse and girder models, is conducted first. The force-deformation curve of the integrated analysis is shown in Figure 6 (a). The impact force increases to a maximum of 23 MN at 0.4 m crush depth and the slope represents the instantaneous stiffness of the front stiffened plate in the deckhouse. As the ship travels further, the edge of the girder starts to deform and thus the impact force ceases to increase and fluctuates around 20 MN. An abrupt drop can be observed at 0.9 m ship deformation. This is associated with rupture initiation in the front plate of the deckhouse. After 1.1 m crush depth, the front plate is torn completely open. After that, the girder only interacts with the vertical side plates and deckhouse internal structures. Hence, a low force level of around 7 MN is observed.

The energy dissipation curves for both structures are shown in Figure 6 (b). As the deckhouse undergoes a much severer damage than the girder, it dissipates the majority of the collision energy. The bridge girder generally remains intact until 0.5 m crush depth. Later, structural deformation occurs in the girder, but less than 20% of the total energy is dissipated by the bridge girder.
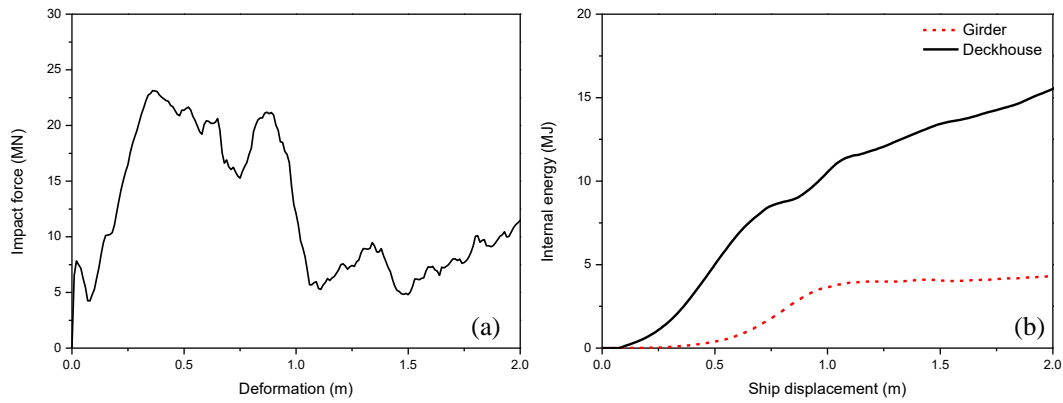
Figure 6. (a) Force-deformation curve and (b) energy dissipation curves of the girder and the deckhouse.

Rigid girder assumption

Due to the large difference in the relative strength of the girder and the deckhouse, major damage occurs in the ship deckhouse while the bridge girder undergoes limited deformations. Hence, a rigid girder simplification may be reasonable. Thus, a rigid girder collision against a deformable deckhouse is simulated. This modelling technique can largely reduce the modelling effort and computational time while yielding an acceptable prediction of impact force. The force-deformation curve and energy dissipation curves are compared with those obtained from the integrated analysis.

As the initial response is controlled by the resistance of the deckhouse, a similar force magnitude and slope can be observed until 0.3 m crush depth. After that, a clear distinction can be observed from the two cases. In the rigid girder case, the force continues to increase as the ship crashes further. This is because the deformation of the deckhouse plate increases. In the integrated analysis, however, the deformation of the girder tip releases the collision force.

Later, the force quickly drops to around 5 MN as the girder penetrates the deckhouse plate in the rigid case. It is interesting to find that the deckhouse plate is penetrated at a later stage when collided by the rigid girder. This is because as the girder

travels further, the deckhouse plate keeps deforming and the curvature increases, which mobilizes the plates and stiffeners in the upper and lower compartments in the deckhouse. In the integrated analysis, the girder deformation releases the collision load due to the deformation of the girder. Therefore, the capacity of the stiffened deckhouse plate is sufficient to resist the collision load and thus the damage is concentrated locally between two horizontal decks. The different deformation patterns are illustrated in Figure 8.

In general, when the girder is assumed rigid, the maximum collision force and structural deformation are slightly overestimated. As shown in Figure 7 (b), the two cases are identical in terms of energy dissipation when the deformation is less than 0.5 m. For a deformation of 2.0 m, 25% more energy is dissipated by the deckhouse by assuming a rigid girder. Nevertheless, considering the significantly reduced modelling and simulation efforts, this conservative rigid girder assumption is acceptable for fast prediction of the collision response of the ship deckhouse in the preliminary design phase.
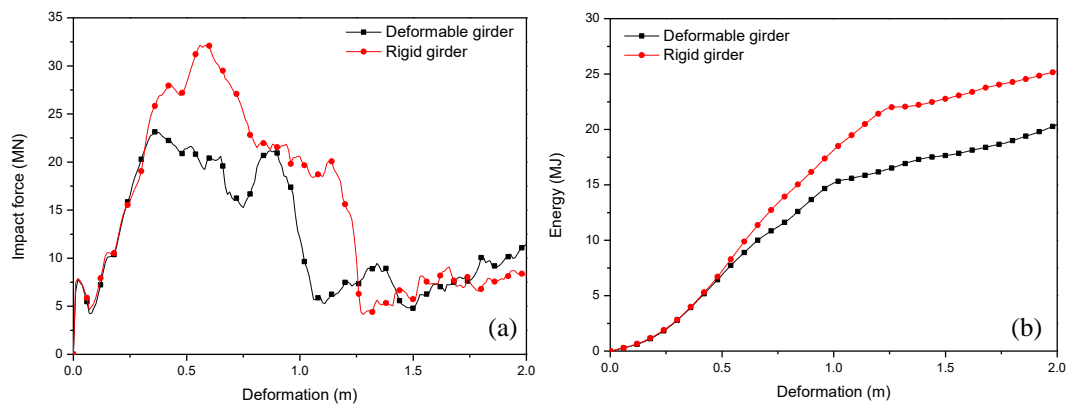

Figure 7. Comparison of force and energy for integrated analysis and rigid girder assumption, (a) force-deformation and (b) energy absorption curves.
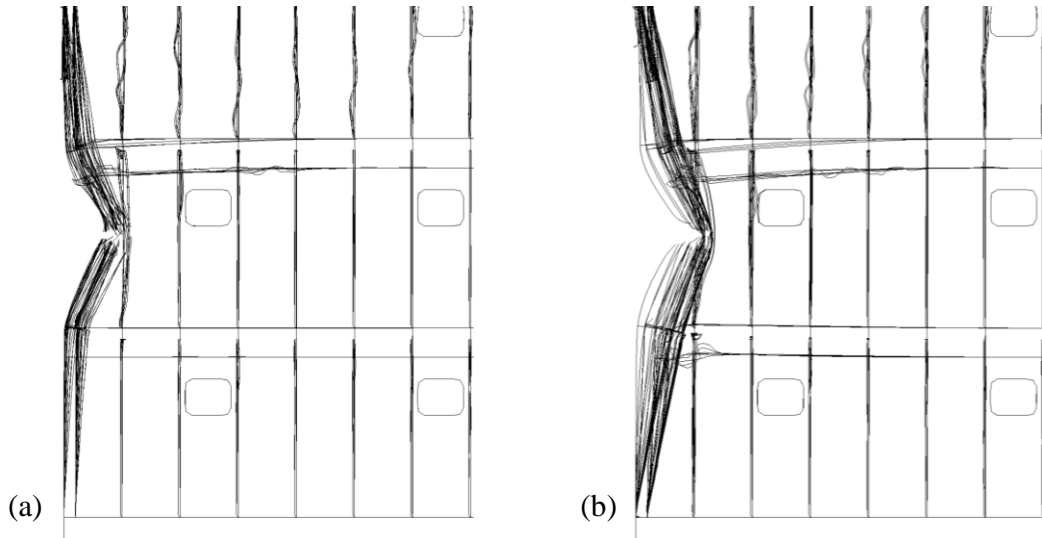
(a)
(b)

Figure 8. Side views of the ship deckhouse deformation at 1 m ship displacement, (a) integrated analysis and (b) rigid girder against deformable deckhouse.

Deckhouse deformation mechanism

The deckhouse deformation process during a deckhouse-girder collision is illustrated in Figure 9 and the deformation of structural components is illustrated in Figure 10. For the investigated deckhouse, the total structural resistance can be obtained by adding up the individual resistance from the following structural components: the front plate, the nineteen stiffeners supporting the front plate, the four vertical side plates and the horizontal decks at each stage.

Based on the deformation pattern, the collision process can be defined as a three-stage deformation mechanism as shown in Figure 9.

Stage 1: Plastic deformation develops in the front plate and the supporting stiffeners. Meanwhile, crushing deformation occurs in the vertical side plates. The structural deformation is localized between two horizontal decks. The total structural resistance is obtained by adding up the membrane deformation of the front plate, the

bending and membrane resistances of the attached stiffeners and the folding deformation of the side vertical plates.

Stage 2: As the ship travels further, the top and bottom horizontal decks may start to fail as they can no longer support the membrane forces in the front plate. When the decks fail, the front plates in the upper and lower compartments are engaged. Rupture starts to initiate from the two side edges of the front plate and propagates towards the centre of the plate. Meanwhile, the vertical side plates suffer continuous tearing failure after the first fold. The structural resistance in this stage includes the membrane deformation of the front plate, the bending and membrane resistances of the attached stiffeners, the folding and possible tearing of the vertical side plates. If the decks are strong, rupture may also initiate before the adjacent horizontal decks fail and lead to early loss of membrane force in the front plate.

Stage 3: When the front plate is completely penetrated, the structural response is dominated by the crushing and bending resistances of the horizontal deck and the tearing of the vertical side plates.
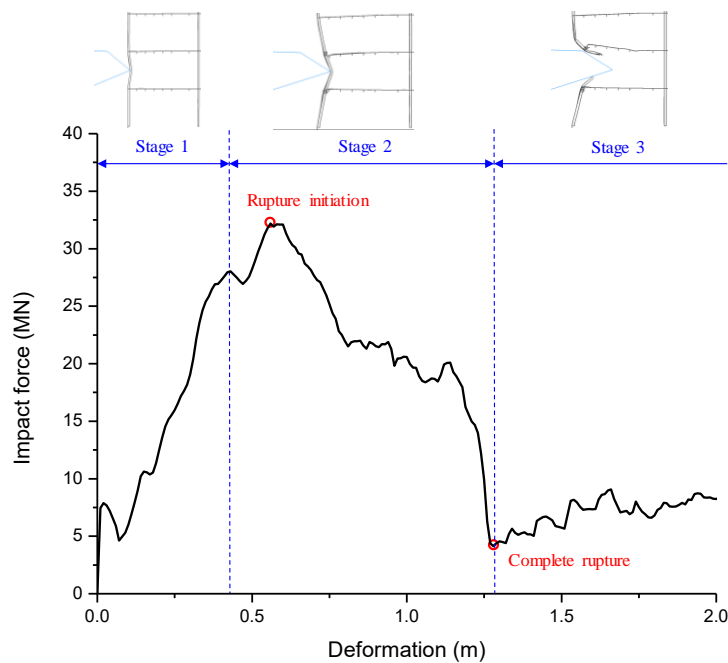
Figure 9. Force-deformation curve of the collision and the corresponding deckhouse deformations for the three stages.
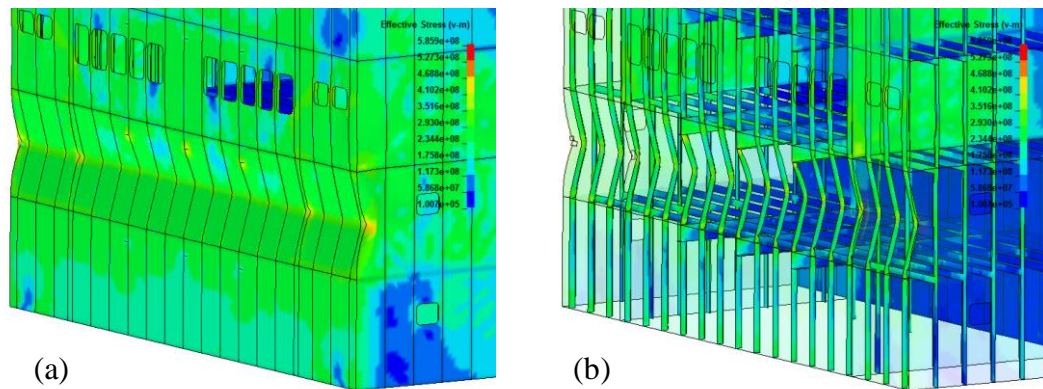

(a) (b)

Figure 10. Illustrations of deckhouse deformation by (a) outer plates and (b) internal structures.

Simplified analytical method

As the numerical method requires an accurate establishment of finite element models and a high demand for computational resources, it is not applicable for the rapid collision assessment in the preliminary design phase. Alternatively, a simple yet accurate analytical method should be used to estimate the impact resistance and energy dissipation in the early design stage.

In a deckhouse-grider collision, the deckhouse will suffer severe plastic deformations, which makes it possible to analytically estimate the structural resistance and energy dissipation associated with these deformations. Analytical plastic methods have been widely used to evaluate the structural resistance and energy dissipation of the structural components in ship-ship collision analyses, typically bow collision with ship side structures (Hong and Amdahl 2012, Liu 2017, Sun, Hu and Wang 2015). In the analysis, it is common to assume the bow of the striking ship is rigid and the side structure of the struck ship is deformable. Further, the structural components of the struck ship are assumed to behave independently, i.e., no coupling is considered among

the structural components (Tabri 2012, Wierzbicki and Driscoll 1995, Wierzbicki and Thomas 1993). Then, analytical formulae can be developed for each structural component, and the total resistance and energy absorption are obtained by simply adding up the contributions of each individual structural component engaged in the collision.

Based on the deformation mechanism discussed in the previous section, a simplified analytical approach is proposed to estimate the resistance of the ship deckhouse when colliding with a bridge girder. The total structural resistance is established by assembling the contributions of the front plate, the stiffeners, the side vertical plates and the horizontal decks.

Response of the front plate

The deformation pattern of the front shell plating from the numerical simulation is shown in Figure 11 (a). It can be idealized as a simplified deformation model as shown in Figure 11 (b). The geometry of the shell plating is illustrated in the figure, where L_1 and L_2 are the distances to the top and bottom horizontal decks, respectively. The corresponding rotational angles are α_1 and α_2, respectively. H_p is the width of the shell plating.
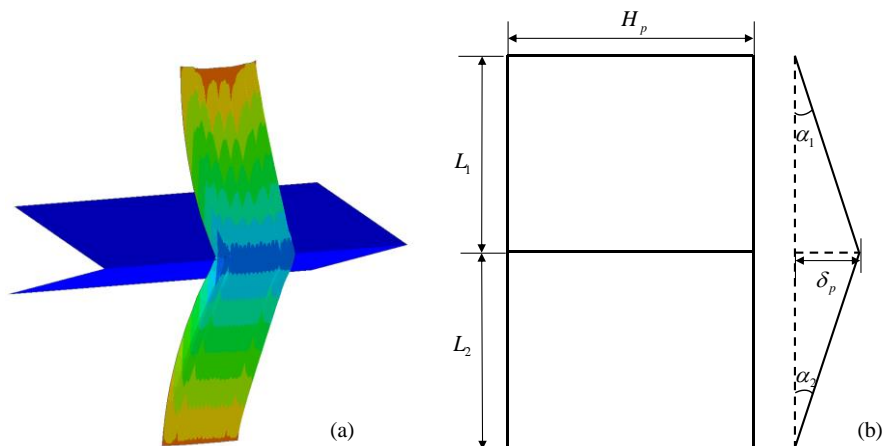

(a)   (b)

Figure 11. Deformation of the front shell plating, (a) numerical and (b) simplified.

The deformation of the plate can be expressed as

$$\delta_p = L_1 \tan \alpha_1 = L_2 \tan \alpha_2 \tag{1}$$

Then, the impact load velocity can be obtained as

$$\dot{\delta}_p = L_1 \frac{\dot{\alpha}_1}{\cos^2 \alpha_1} = L_2 \frac{\dot{\alpha}_2}{\cos^2 \alpha_2} \tag{2}$$

where $\dot{\alpha}_1$ and $\dot{\alpha}_2$ are the angular bending rates of the top and bottom plates.

The strain rates of the top and bottom plates can be obtained by

$$\dot{\varepsilon}_{p1} = \frac{\sin \alpha_1}{\cos^2 \alpha_1} \dot{\alpha}_1 \tag{3}$$

$$\dot{\varepsilon}_{p2} = \frac{\sin \alpha_2}{\cos^2 \alpha_2} \dot{\alpha}_2 \tag{4}$$

As the plate suffers a large plastic deformation, the proportion of the bending energy dissipation is small (Sun, Hu and Wang 2017). Thus, the bending resistance of the plate is neglected and only the membrane energy dissipation is considered. The membrane energy dissipation rate $\dot{E}_m$ of the front plate can be obtained by

$$\dot{E}_m = \int_S N_p \dot{\varepsilon}_{pi} dS \tag{5}$$

where N_p is the plastic membrane force. $\dot{\varepsilon}_{pi}$ is the average tensile strain rate and S is the plate area. The material is assumed to be rigid-perfectly plastic and the

elastic strain is neglected. A flow stress σ_0 which is computed by the average value of the yield stress σ_y and the ultimate stress σ_u is used to consider the material hardening.

By integrating Equations 3 and 4 into Equation 5, the dissipation rate of the membrane energy can be expressed as

$$\dot{E}_m = \sigma_0 t_p (S_1 \frac{\sin \alpha_1}{\cos^2 \alpha_1} \dot{\alpha}_1 + S_2 \frac{\sin \alpha_2}{\cos^2 \alpha_2} \dot{\alpha}_2) \tag{6}$$

where t_p is the thickness of the front shell plating. S_1 and S_2 are the area of the top and bottom plates which can be expressed by $S_1 = H_p \cdot L_1$ and $S_2 = H_p \cdot L_2$, respectively.

According to the 'upper-bound theorem' (Jones 2011), the instantaneous force can be derived by equating the rate of external work with the rate of internal energy dissipation. It can be expressed as

$$F \cdot \dot{\delta} = \dot{E}_i \tag{7}$$

where F is the plastic force which equals the external collision load. $\dot{\delta}$ is the crushing velocity. $\dot{E}_i$ is the internal strain energy dissipation rate.

Combining Equations 2, 6 and 7, the resistance of the front shell plating can be obtained by

$$F_p = \frac{\dot{E}_m}{\dot{\delta}_p} = \sigma_0 t_p (\frac{S_1 \sin \alpha_1}{L_1} + \frac{S_2 \sin \alpha_2}{L_2}) = \sigma_0 t_p H_p (\sin \alpha_1 + \sin \alpha_2) \tag{8}$$

This maximum deformation δ_m can be estimated by a strain-based criterion as expressed by

$$\delta_m = L_{\min} \sqrt{\varepsilon_m^2 + 2\varepsilon_m} \tag{9}$$

where $L_{\min}$ is the smaller one of the two plate height separated by the girder. ε_m is the critical strain. As suggested by Amdahl (Amdahl 1995), this critical strain should be taken between 0.05 and 0.1 for full-scale collision assessment. In this work we have assumed the critical strain to be 0.05.

During collision, large plastic deformations and membrane forces develop at the contact area on the front plate. It is observed that for the plate with a large width (14.7 m), rupture is not initiated simultaneously throughout the plate width. Large plastic strain initiates the rupture of the front plate from the two sides. Later, the crack propagates towards the centre of the plate along the contact line with the girder edge as shown in Figure 12. This phenomenon is considered by a rupture propagation coefficient k_{rp}, which can be obtained by

$$k_{rp} = \begin{cases} 1 & n \leq \lambda_{rp} \\ 1 - \dfrac{n - \lambda_{rp}}{100 - \lambda_{rp}} & \lambda_{rp} < n \leq 100 \end{cases} \tag{10}$$

The parameter λ_{rp} in the above equation is an integer accounting for the vertical distance to the closest deck. This location coefficient λ_{rp} can be obtained by

$$\lambda_{rp} = \left\lfloor 100(1 - \frac{L_{\min}}{L/2}) \right\rfloor \tag{11}$$
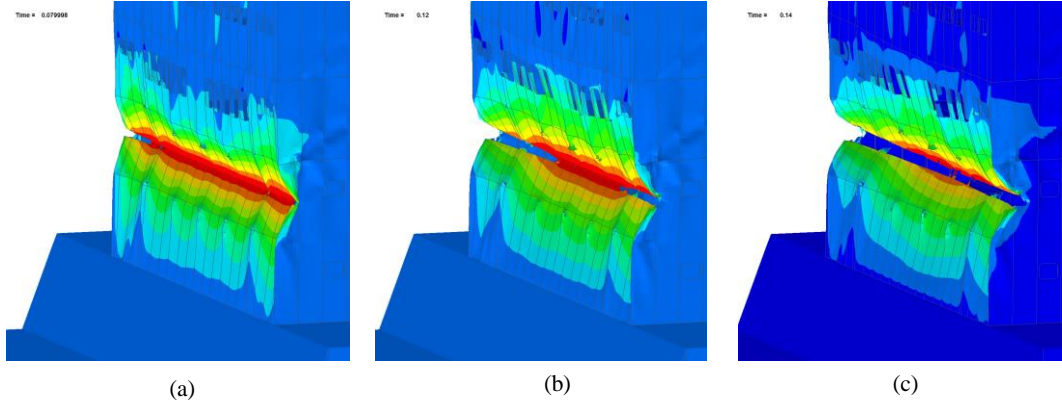
<center>(a)　　　　　　　　　(b)　　　　　　　　　(c)</center>

Figure 12. Rupture process of the front plate.

Response of the Stiffeners

The numerically obtained response of the stiffener attached to the front shell plating is shown in Figure 13 (a). Based on this deformation pattern, a simplified model is proposed as shown in Figure 13 (b). It is assumed that the length and rotational angle of the stiffeners are identical to those of the attached front shell plating. The energy dissipated by the plastic bending of stiffeners at both sides can be obtained by

$$\dot{E}_{s1} = M_{s0} t_s (\dot{\alpha}_1 + \dot{\alpha}_2) \tag{12}$$

where M_{s0} is the full plastic bending moment per thickness of the stiffeners. t_s is the thickness of the stiffeners.

In the impacted area, the collision energy is dissipated through plastic bending and membrane stretching. The energy dissipation rate can be obtained by

$$\dot{E}_{s2} = M_{s1} t_{s1} \dot{\alpha}_1 + M_{s2} t_{s2} \dot{\alpha}_2 + N_{s1} t_{s1} \dot{\varepsilon}_{s1} + N_{s2} t_{s2} \dot{\varepsilon}_{s2} \tag{13}$$

By using the interaction criterion and the normality criterion (Jones 2011), the normal force can be expressed as

$$N = \frac{N_{s0}^2}{2M_{s0}} \cdot \frac{\dot{\varepsilon}_s}{\dot{\alpha}} \qquad (14)$$

The total energy dissipation by the stiffeners can be obtained by combining Equations 12-14 as

$$\dot{E}_s = \dot{E}_{s1} + \dot{E}_{s2} = 2M_{s0}t_s(\dot{\alpha}_1 + \dot{\alpha}_2) + \frac{N_{s0}}{M_{s0}}t_s(\frac{\sin^2\alpha_1}{\cos^4\alpha_1}\dot{\alpha}_1 + \frac{\sin^2\alpha_2}{\cos^4\alpha_2}\dot{\alpha}_2) \qquad (15)$$

Then, the resistance force is

$$F_s = \frac{\dot{E}_s}{\dot{\delta}_s} = \frac{1}{2}\sigma_0 H_s t_s(\frac{\cos^2\alpha_1}{L_1} + \frac{\cos^2\alpha_2}{L_2}) + 4\sigma_0 H_s t_s(\frac{\sin^2\alpha_1}{\cos^2\alpha_1 L_1} + \frac{\sin^2\alpha_2}{\cos^2\alpha_2 L_2}) \qquad (16)$$
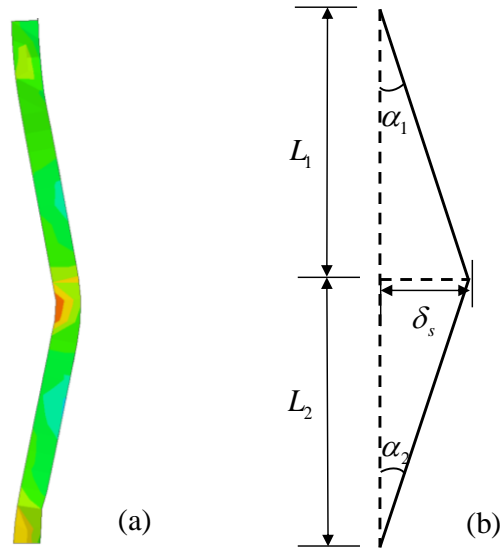

Figure 13. Deformation of the stiffeners, (a) numerical and (b) simplified.

Response of the vertical side plates

In the vertical direction, there are four side plates which support the deckhouse. These plates will also get in contact with the bridge girder. Therefore, the resistance of the vertical side plates should also be accounted for.

A typical deformation pattern of the vertical plates is shown in Figure 14 (a). This response is similar to the girder crushing response of the ship side structures (Hong and Amdahl 2008, Simonsen 1997, Wang and Ohtsubo 1997, Zhang 1999). Simplified models have been developed by the various authors based on different folding mechanisms (Hong and Amdahl 2008). According to the deformation pattern observed from the numerical simulation, the response of the side plates can be divided into two stages: (1) the fold with a $2H_g$ folding length, and (2) the tearing after the fold.

For the first stage, the folding length of the side plates can be obtained by the following equation according to Zhang (Zhang 1999):

$$H_g = 0.8383(L_1 L_2 t_g)^{1/3} \tag{17}$$

As summarized by Hong and Amdahl (Hong and Amdahl 2008), the proposed formulations are able to predict the mean crushing force for the web girders as it is largely dependent on the plate slenderness ratio. In this study, the resistance of the vertical side plates is calculated by (Zhang 1999)

$$F_g = 0.631\sigma_0 t^{1.83} \frac{L_1 + L_2}{(L_1 L_2)^{0.17} \delta_g^{0.5}} + 0.645\sigma_0 t^{1.33} \delta_g \frac{L_1 + L_2}{(L_1 L_2)^{0.67}} \tag{18}$$

where the deformation of the vertical plate δ_g is identical to δ_p .

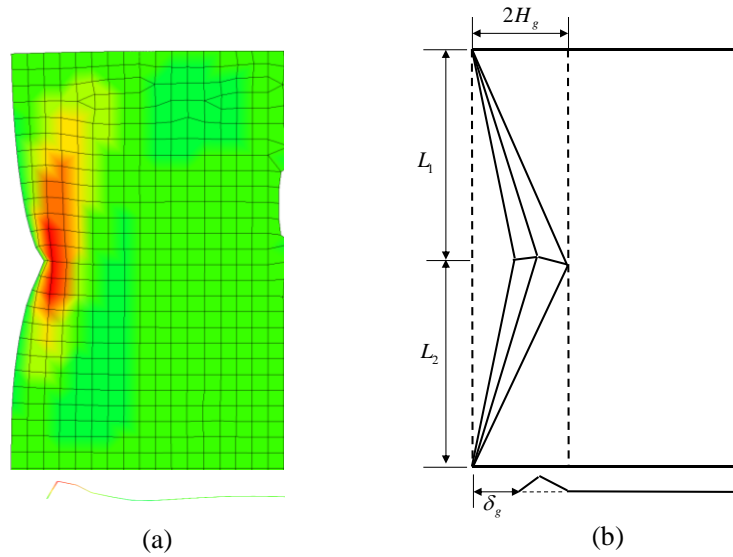(a)   (b)

Figure 14. Crushing deformation of the vertical side plate, (a) numerical and (b) simplified.

After the fold, the sharp girder edge penetrates into the side vertical plates and initiates the tearing failure as shown in Figure 15. The tearing resistance of the vertical plate can be expressed by (Sun, Hu and Wang 2015)

$$F_{\mathrm{w}} = 1.942\sigma_0 t_{\mathrm{g}}^{1.5} \delta_{\mathrm{g}}^{0.5} \varepsilon_{rg}^{0.25} (\tan\beta)^{0.5} (1 + \frac{\mu}{\tan\beta}) \tag{19}$$
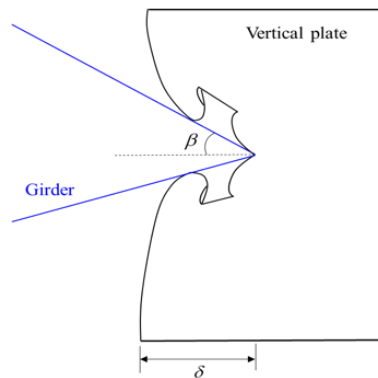

Figure 15. Tearing damage model of the vertical side plate.

Response of the horizontal decks

The horizontal decks will also engage in the collision if the girder gets in contact with

the deckhouse at a position close to the horizontal decks. As shown in Figure 16, the deformation procedure of the horizontal deck can be divided into two stages: the crushing of the front part and the membrane deformation of the remaining part. Similar to a girder response in a grounding accident, the crushing resistance of a horizontal deck can be obtained by (Hong and Amdahl 2012)

$$F_{dc} = M_{d0} \frac{4}{R}(2C) \qquad (20)$$

where M_{d0} is the full plastic bending moment of the deck. R is the rolling radius (here taken equal to the distance from the lower deck to the girder bottom and C is the length of the deck.

For the collision scenario in which the girder edge is close to one of the horizontal decks, a membrane resistance due to the girder vertical pushing should also be included. Similar to the front shell plating, this membrane resistance of the horizontal decks F_{dm} under a vertical load is obtained by equating the external work with the internal membrane energy as

$$F_{dm} = \sigma_0 t_d H_d (\sin \gamma), \qquad (21)$$

where t_d and H_d are the thickness and width of the horizontal deck. γ is the rotational angle as of the deck.
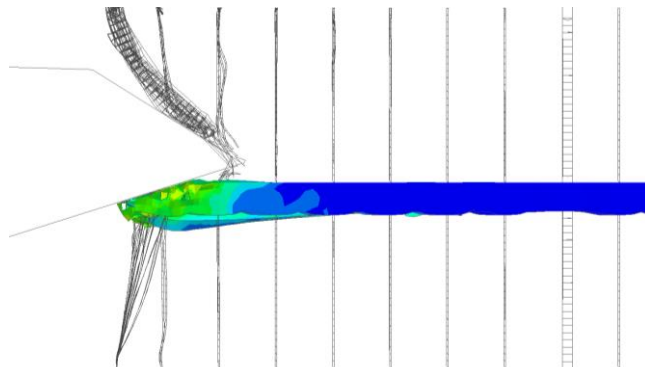
Figure 16. Deformation of the horizontal deck.

Application and verification of the proposed analytical method

Application of the analytical method

With the above-derived equations, the total deckhouse resistance and energy absorption can be obtained by assembling the contributions from the involved structural members at each stage. The maximum deformation of each stage is determined from Equation 9 where the critical strain and the minimum distance to the upper/lower deck are important parameters. Specifically, the end of the first stage is determined by the smaller distance to the upper/lower deck and the end of the second stage is determined by the smaller distance to the next (adjacent) upper/lower decks. The typical illustration of deckhouse deformation in each stage is shown in Figure 17.

Stage 1   Stage 2   Stage 3
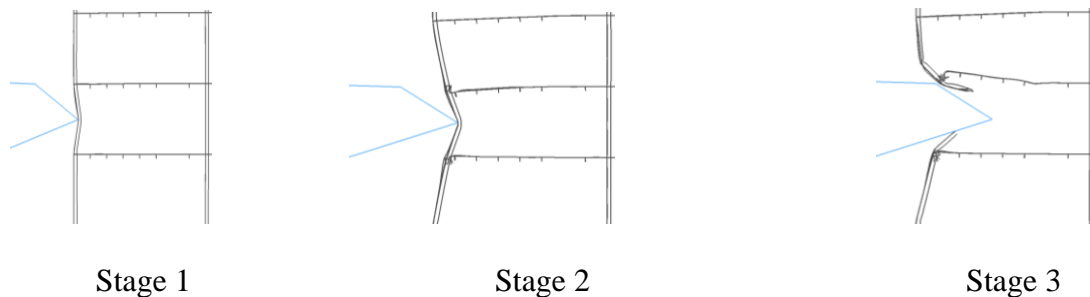
Figure 17. Illustrations of the typical deformation mechanisms for the three stages.

An example case is given here to illustrate the application of the analytical method. The bridge girder is assumed to collide with the ship deckhouse at Location 3 as shown in Figure 18.

Stage 1: $0 \leq \delta_m \leq 0.096$ m. In this stage, the deformation only occurs within one deck level. The end of the stage is determined by Equation 9 for $L_m = 0.3$ m which is the smaller distance to the upper (2.3 m) / lower (0.3 m) decks. The critical strain ε_m is assumed to be 0.05.

The resistance of the front plating (Equation 8) and its stiffeners (Equation 16) at the impacted sections contributes to the impact resistance. For the vertical side plates, the folding resistance (Equation 18) is first used and the tearing resistance (Equation 19) should apply after the crush depth exceeds the folding length calculated from Equation 17.

Stage 2: $0.096 \text{ m} < \delta_m \leq 0.928 \text{ m}$. In this stage, the upper and lower decks are involved, and later rupture starts to initiate at the font plating until the front plate is completely torn open. The end of the stage is obtained by Equation 9 for $L_m = 2.9 \text{ m}$ which is the smaller distance to the adjacent upper (2.3+2.6=4.9 m) / lower (0.3+2.6=2.9 m) decks.

The resistance of the front plating is obtained by Equation 8 times the rupture propagation coefficient in Eq. 10. The resistance of the attached stiffeners (Equation 16) and the folding (Equation 18) and tearing (Equation 19) resistances of the vertical side plates also contribute to the total resistance.

Stage 3. $\delta_m > 0.928 \text{ m}$. The front plate is completely penetrated and thus there is no resistance contribution from the front plate and its stiffeners. The tearing resistance of the vertical side plates remains and can be calculated by Equation 19. In this stage, the crushing (Equation 20) and the bending (Equation 21) resistances of the horizontal deck also contribute to the total resistance.

With the above calculated structural resistance in each stage, the corresponding energy dissipation is obtained by integrating the structural resistance with the crush depth.
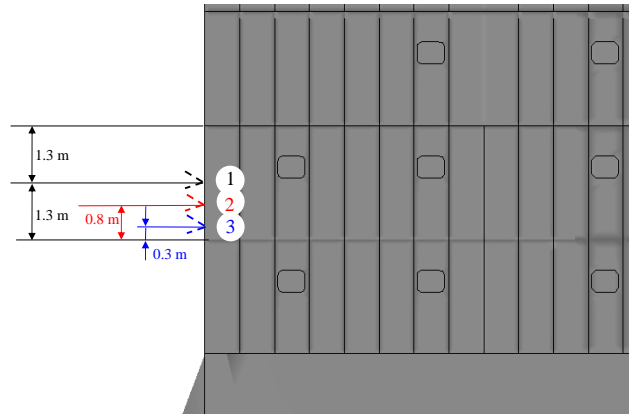
Figure 18. Illustration of the three impact heights.

Method validation

To verify the simplified method, the force-deformation and energy dissipation curves are compared with the results from numerical simulations. The sensitivity of the impact location is evaluated by varying the girder impact height as shown in Figure 18.

In case 1, the girder collides with the deckhouse in the middle of two horizontal decks. In the first stage, the front plate, the stiffeners and the vertical side plates between the two decks are engaged in the collision. As shown in Figure 19, the analytical method predicts a first major peak force of 25.7 MN at 0.42 m which is quite close to the 27.9 MN force at 0.43 m deformation obtained in the numerical simulation. In the second stage, the front plate and stiffeners in the upper and lower compartments are engaged in the collision as shown in Figure 8 (b). The analytical method predicts plate rupture initiation at 0.58 m deformation, which is virtually identical to 0.56 m in the numerical simulation. The drastic drop in the resistance curve after the peak value is due to the complete rupture of the front plate and the attached stiffeners. Later, the main contributions to the resistance stem from tearing of the vertical side plates and crushing of the horizontal decks. The folding length of the side plates is 0.6 m according to

Equation 17. The tearing resistance dominates the response of the side plates after the first fold.

In case 2, the girder collides with the deckhouse closer to the deck below. Therefore, the rupture of the front plate and the attached stiffeners occurs earlier than in case 1. This behaviour is well captured by the analytical method as shown in Figure 20 (a). The overall force level is also lower than that in case 1, but the response is generally similar to case 1.

In case 3, the girder impact location is only 0.3 m from the lower deck. Consequently, the front plate and the stiffeners fail at the smallest deformation level. The plating in the deck engages in the collision at an early stage. The front plate is completely torn apart at 0.7 m deformation, which is much smaller than the other two cases (see Figure 21). After about 1 m deformation, the horizontal deck suffers from vertical bending. The associated membrane resistance is included in stage 3 by Equation 21.

The energy absorption curves of the three cases are compared in Figures. 19-21 (b). It is found that the energy estimation by the simplified analytical method is comparable to the numerical prediction. In all cases complete rupture of the front plate has a tremendous impact on the resistance, and rupture is quite accurately predicted. For the collision scenario with an impact location close to the horizontal deck, the stiffened plate fails earlier and thus a lower energy absorption capability is observed. The location of impact has a significant influence on the collision resistance of the deckhouse. When the impact location is close to the horizontal decks, the impact resistance is relatively low because of early rupture initiation.
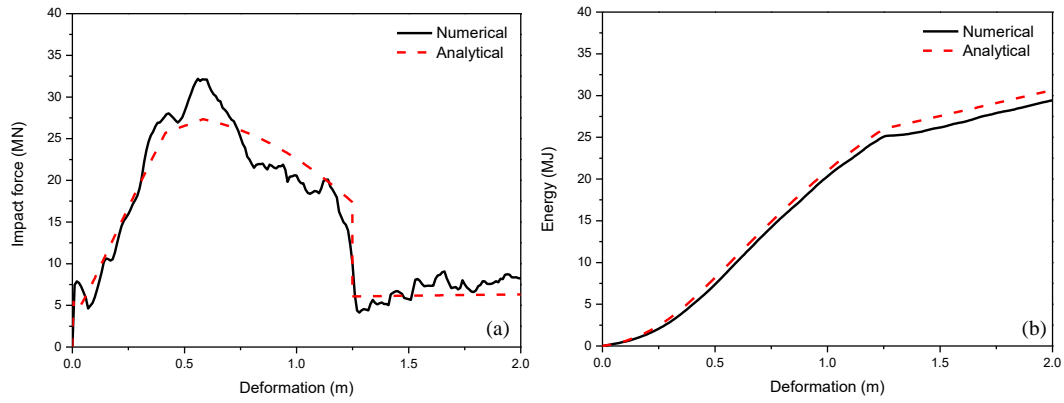
Figure 19. Comparison between the numerical and analytical methods for case 1, (a) force-deformation curves and (b) energy-deformation curves.
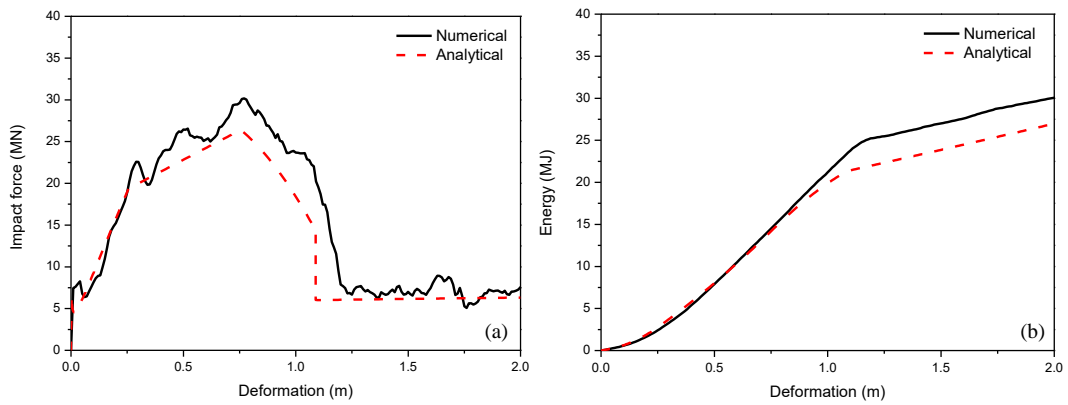

Figure 20. Comparison between the numerical and analytical methods for case 2, (a) force-deformation curves and (b) energy-deformation curves.
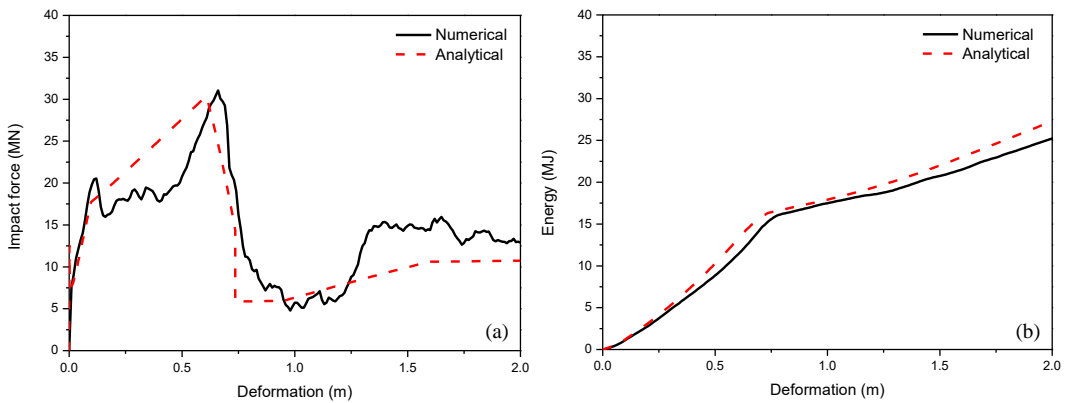

Figure 21. Comparison between the numerical and analytical methods for case 3, (a) force-deformation curves and (b) energy-deformation curves.

To further validate the proposed simplified method, a finite element deckhouse with increased plate and stiffener thicknesses (case 4) was modelled. The thicknesses of

the original and increased plates and stiffeners are listed in Table 2. The resistance and energy dissipation obtained with the analytical and numerical methods for the new model (case 4) are compared in Figure 22. In general, the agreement is good.

Table 2. Plate and stiffener thicknesses.

Structural component	Case 1	Case 4
Front plate	9.5 mm	12 mm
Stiffener	7 mm	10 mm
Vertical side plate	8 mm	12 mm

In case 4 the deformation pattern is slightly different from that of case 1. As the thickness increases, the strength of the stiffened front plate increases. The initial slope of the resistance curve is steeper and the resistance at the end of the first stage is also higher. The structural components in the upper and lower compartment engage earlier in the collision. Therefore, the deformation at the end of the first stage is smaller than that in case 1 (0.35 m versus 0.45 m). Later, the deformation (1.1 m) at complete rupture of the front plate is also smaller than that of Case 1 (1.25 m) as a thicker stiffened plate is less ductile. The overall force level in case 4 is, however, somewhat larger than that in case 1.
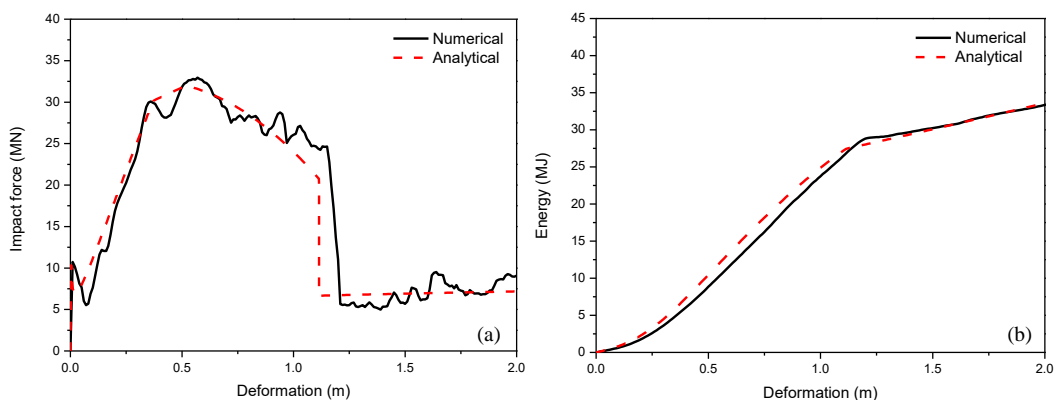

Figure 22. Comparison between the numerical and analytical methods for thicker deckhouse components (case 4), (a) force-deformation curves and (b) energy-deformation curves.

Conclusions

In this study, finite element models of a container ship deckhouse and a bridge girder section were developed. Numerical simulations were conducted to investigate the response of deckhouse-girder collisions. It was found that the bridge girder, which has a higher strength, only endured minor deformations while the relatively weaker deckhouse suffered excessive damages. A rigid girder assumption may yield acceptable prediction accuracy for fast estimation in the preliminary analysis stage.

Based on the observation of the deformation pattern in the numerical simulations, a new simplified analytical method is proposed to predict the structural resistance and energy absorption of a ship deckhouse colliding with bridge girders. The overall response of the deckhouse is obtained by adding up the individual responses of the front plate, the stiffeners, the side plates, and the horizontal decks. The resistance models for these components, are to a large extent, based upon existing models for ship substructures subjected to grounding and collisions.

Three bridge girder-ship deckhouse impact scenarios were considered using the proposed analytical method. The estimated structural resistance and energy absorption were compared with the results from the numerical simulations. Good agreement between the analytical and numerical method was obtained.

The analytical method is useful for estimating the collision response of large stiffened panels subjected to through-span impact loads, such as in deckhouse-girder collisions. The main advantage of the analytical method is that it can be efficiently used for fast parametric analysis in the early design stages (different impact locations and structural dimensions etc.).

Acknowledgements

References

Alsos HS, Amdahl J, Hopperstad OS. 2009. On the resistance to penetration of stiffened plates, Part II: Numerical analysis. International Journal of Impact Engineering.36:875-887.

Amdahl J. 1995. Side collision. 22nd WEGEMT Graduate School, Technical University of Denmark.

Hong L, Amdahl J. 2008. Crushing resistance of web girders in ship collision and grounding. Marine Structures.21:374-401.

Hong L, Amdahl J. 2012. Rapid assessment of ship grounding over large contact surfaces. Ships and Offshore Structures.7:5-19.

Jones N. 2011. Structural impact: Cambridge university press.

Larsen OD. 1993. Ship collision with bridges: The interaction between vessel traffic and bridge structures: IABSE.

Liu B. 2017. Analytical method to assess double-hull ship structures subjected to bulbous bow collision. Ocean Engineering.142:27-38.

Sha Y, Amdahl J. Design of Floating Bridge Girders against Accidental Ship Collision Loads. Proceedings of the The 19th Congress of IABSE; 2016.

Sha Y, Amdahl J. Ship Collision Analysis of a Floating Bridge in Ferry-Free E39 Project. Proceedings of the 36th International Conference on Ocean, Offshore and Arctic Engineering; 2017: American Society of Mechanical Engineers.

Sha Y, Amdahl J, Dørum C. 2018. Local and global responses of a floating bridge under ship-girder collisions. Journal of Offshore Mechanics and Arctic Engineering.

Sha Y, Hao H. 2012. Nonlinear finite element analysis of barge collision with a single bridge pier. Engineering Structures.41:63-76.

Sha Y, Hao H. 2014. A simplified approach for predicting bridge pier responses subjected to barge impact loading. Advances in Structural Engineering.17:11-23.

Simonsen BC. 1997. Ship grounding on rock—I. Theory. marine Structures.10:519-562.

Storheim M, Amdahl J. 2017. On the sensitivity to work hardening and strain-rate effects in nonlinear FEM analysis of ship collisions. Ships and Offshore Structures.12:100-115.

Sun B, Hu Z, Wang G. 2015. An analytical method for predicting the ship side structure response in raked bow collisions. Marine Structures.41:288-311.

Sun B, Hu Z, Wang J. 2017. Bottom structural response prediction for ship-powered grounding over rock-type seabed obstructions. Marine Structures.54:127-143.

Tabri K. 2012. Influence of coupling in the prediction of ship collision damage. Ships and Offshore Structures.7:47-54.

Wang G, Ohtsubo H. Deformation of ship plate subjected to very large load. Proceedings of the Proceedings of the international conference on offshore mechanics and arctic engineering; 1997: American Society of Mechanical Engineers.

Wierzbicki T, Driscoll JC. 1995. Crushing damage of web girders under localized static loads. Journal of Constructional Steel Research.33:199-235.

Wierzbicki T, Thomas P. 1993. Closed-form solution for wedge cutting force through thin metal sheets. International Journal of Mechanical Sciences.35:209-229.

Zhang S. 1999. The mechanics of ship collisions: Institute of Naval Architecture and Offshore Engineering.

Zhang S, Pedersen PT. 1999. The mechanics of ship collisions.